Journal of Applied Polymer Science

α-Cyclodextrin Assisted Self-Assembly of Poly(ethylene glycol)-block-Poly(*N*-isopropylacrylamide) in Aqueous Media

Fanny Yuen, Kam Chiu Tam
Department of Chemical Engineering and Waterloo Institute for Nanotechnology, University of Waterloo, Waterloo, Ontario, Canada N2L 3G1
Correspondence to: K. C. Tam (E-mail: mkctam@uwaterloo.ca)

ABSTRACT: Poly(ethylene glycol)-block-poly(*N*-isopropylacrylamide) (PEG-*b*-PNIPAM) block copolymers were synthesized by atom transfer radical polymerization, and the α-cyclodextrin (α-CD) induced self-assembly characteristics of the system were elucidated. Below the lower critical solution temperature (LCST) of PNIPAM, CD threaded onto the PEG segments and induced micellization to form rod-shaped nanostructures comprising of a PEG/α-CD condensed phase and a PNIPAM shell. Increasing the temperature of system above the LCST caused the PNIPAM segments to collapse, which resulted in the dethreading of the CD. © 2012 Wiley Periodicals, Inc. J. Appl. Polym. Sci. 000: 000–000, 2012

KEYWORDS: cyclodextrin; block copolymers; self-assembly; inclusion complexes; atom transfer radical polymerization

Received 13 June 2011; accepted 3 May 2012; published online
DOI: 10.1002/app.38072

INTRODUCTION

Supramolecular self-assemblies have the ability to produce well-defined architectures with tailored physical properties.[1,2] Self-assemblies consist of dynamic noncovalent interactions.[3] Block copolymers composed of hydrophilic and hydrophobic blocks are able to spontaneously self-assemble into various ordered micellar structures.[4,5] The polymers self-organize into assembled nanostructures which sequester the hydrophobic segments and form hydrophilic shell that enhance the stability of the system in aqueous media. These polymeric micelles have attracted the attention of the scientific community due to their potential applications in controlled drug delivery.[6–9] The most common micellar morphologies include spherical-, cylindrical-, and vesicle-shaped micelles. The size and shape of these micelles are dependent on the curvature between the condensed and extended phases.[10]

Poly(ethylene glycol) (PEG) is a biocompatible polymer that is FDA approved for biomedical applications,[11,12] and PEG-containing Pluronics are commercially available as drug delivery vehicles.[13,14] PEG can increase the biocompatibility of synthetic materials due to its good solubility in water and minimal interfacial energy.[15] The grafting of hydrophobic blocks to PEG has been widely studied and applied to a variety of potential applications in biomedical and specialty chemicals sectors. In dilute solutions of poly(ethylene oxide)-*b*-polystyrene, regular core-shell micelles were found to coexist with polymeric clusters,[16] and Yu and Eisenberg[17] were able to tailor the block compositions and preparation methods to achieve a variety of morphologies. For use in drug delivery systems, Dai et al.[18] combined poly(ethyl acrylate) with PEG to form a micelle with moderate hydrophobic characteristics and dynamic and permeable cores. Alexandridis and Hatton[19] studied Pluronic triblock copolymers composed of PEG and poly(propylene glycol) (PPG) that were used as polymeric surfactants. In experiments exceeding the critical micelle temperature and critical micelle concentration, micelles comprising of a hydrophobic PPG core and a hydrophilic PEG corona formed in aqueous solution. By varying the composition of ethylene glycol and propylene glycol blocks, the solution and phase behaviors could be manipulated.

Poly(*N*-isopropylacrylamide) (PNIPAM) is a thermo-responsive polymer that exhibits a coil-globule transition in aqueous solution at its lower critical solution temperature (LCST) of approximately 32°C.[20] Below the LCST, PNIPAM is soluble in water. Above the LCST, PNIPAM undergoes a reversible phase transition from a swollen hydrated state to a shrunken dehydrated state, losing ~90% of its volume. PNIPAM has been used in a variety of applications related to temperature-dependent controlled release systems.[21,22]

At low temperatures, PEG-*b*-PNIPAM is highly soluble. At elevated temperatures, the thermo-sensitive PNIPAM block phase separates, and the copolymer self-assembles into various micellar morphologies comprising a PNIPAM core and a hydrophilic

Additional Supporting Information may be found in the online version of this article.

PEG shell.[23–26] Qin et al.[27] discussed the use of PEG-*b*-PNIPAM self-assembled structures as drug delivery vehicles since the polymer was biocompatible. Their PEG-*b*-PNIPAM was found to be amphiphilic in water at body temperature (37°C), and the polymer formed vesicles. However, if the temperature was decreased, the vesicles disassembled and released the encapsulants.

Cyclodextrins (CDs) are a family of cyclic oligosaccharides, α-, *β*-, and *γ*-CD, comprised of 6, 7, and 8 glucose units, respectively, and they are produced by enzymatic conversion from starch. The cavity of the torus-shaped CD allows it to spontaneously complex with a variety of guest molecules to form inclusion complexes (ICs).[28] The driving forces of IC formation between the CD cavity and the guest molecule include geometric compatibility, van der Waals forces, and hydrophobic interactions.[29,30] To stabilize the ICs, hydrogen bonding may occur between the CD and guest molecule and between hydroxyl groups on the rims of neighboring CDs.[31] The formation of these ICs greatly modifies the physical and chemical properties of guest molecules.

Polymer ICs are useful building blocks for constructing supramolecular structures and have been widely studied due to their interesting properties and varied applications.[32] Harada and Kamachi[33] were the first to report the complexation of CD with water-soluble polymers. In their study of α-CD and PEG, they determined that hydrogen bonding was the main factor for IC formation. Through molecular models, they showed that PEG chains were able to penetrate the α-CD cavities while bulkier polymers were not able to. Huang et al.[34] confirmed these results by using a double hydrophilic block copolymer composed of PEG and poly((dimethylamino)ethyl methacrylate) (PDMA). They found that multiple α-CDs threaded onto the PEG chains to form pesudopolyrotaxanes, which then aggregated into novel supramolecular nanostructures. Such aggregation was the driving force for the block copolymer assembly into micellar-like particles comprising of a α-CD/PEG core and a PDMA shell. Block-selective complexation of block copolymers can enhance the amphiphilicity of these block copolymers and enable them to form complex supramolecular structures.

Stimuli-sensitive copolymers with IC capabilities are extremely interesting because they have the ability to form hierarchical self-assembled structures with multiple control elements and have found potential applications in biomedical and nanotechnologies.[35] Liu et al.[36] studied the encapsulation of a double hydrophilic block copolymer composed of PEG and poly(acrylic acid) (PAA) with α-CD at basic pH values. The ICs induced self-assembly into vesicle nanostructures. At low pH, the PAA segments protonated, and the polymer/CD complexes aggregated to produce a turbid solution. Yuan and Shuai[37] developed a PEG-*b*-poly(L-lysine) polymer that exhibited block-specific threading of α-CD to PEG which resulted in supramolecular micellization. Reversible gelation could then be induced by pH change. Duan et al.[38] used ATRP to synthesize a PNIPAM polymer with an insoluble pyrene end group. At low temperatures, the solution was clear due to the formation of micelles. At high temperatures, the solution became turbid as the PNIPAM chains collapsed and agglomerated due to the increased hydrophobicity. *β*-CD is known to form ICs with pyrene. It was found that *β*-CD with pyrene functional groups disturbed the formation of PNIPAM aggregates, resulting in an increase in the system's LCST. Tu et al.[39] synthesized a well-defined PEG-*b*-PNIPAM block copolymer using ATRP. α-CD was added for selective threading of PEG block to transform the system from a random coil to an organized structure. In the solid state, the ICs self-assembled into hexagonally packed plates, and the uncomplexed PEG and PNIPAM chains formed a brush conformation. The system phase separated into alternating long-range-ordered lamellar and amorphous phases.

Supramolecular self-assembly of stimuli-sensitive CD polymeric inclusion complexes are capable of forming a multitude of sophisticated superstructures. PEG-*b*-PNIPAM is double hydrophilic block copolymer that exists as free chains in aqueous solutions at room temperature. However, PNIPAM is temperature sensitive and PEG may be encapsulated by α-CD. When these properties are activated, either separately or together, the hydrophilic/hydrophobic balance of the systems is altered and it can cause the polymer chains to self-assemble. The morphological changes of these self-assembled nanostructures over temperature and complexation in aqueous media is the focus of this study.

MATERIALS AND METHODS

Materials

Poly(ethylene glycol) methyl ether (98.5% purity, MW = 4 970, PDI = 1.04), *N*-isopropylacrylamide (NIPAM, 97%), 2-bromoisobutyryl bromide (98%), copper (I) bromide (CuBr, 99.999%), and isopropyl alcohol (99.5%) were purchased from Sigma Aldrich. Tris(2-aminoethyl)amine (TREN, 96%) was purchased from ACROS Organics. Triethylamine (99%), formic acid (98%), formaldehyde solution (37%), hydrochloric acid (HCl, PUR), and hexane (99.95%), were purchased from Fisher Scientific. Sodium hydroxide (NaOH), methanol (99.8%), methylene chloride (99.5%), and tetrahydrofuran (THF, reagent grade) were purchased from Caledon Lab Chemicals. Benzene (ACS grade) was purchased from EMD Chemicals. HPLC grade toluene (99.9+ %) was purchased from Honeywell. Argon (99.998% oxygen free) was purchased from Praxair. Poly(ethylene glycol) methyl ether and NIPAM were stored in the refrigerator. Water was purified through a Millipore Milli-Q Advantage System.

Polymer Synthesis: Synthesis of PEG macroinitiator, tris(2-(dimethylamino)ethyl)amine (Me_6TREN,) and PEG-*b*-PNIPAM

The synthesis of PEG macroinitator was performed according to the scheme shown in Supporting Information Figure S1,[26] the synthesis of Me_6TREN was done according to the method used by Feng et al.,[40] and the synthesis of the PEG-*b*-PNIPAM was performed by atom transfer radical polymerization (ATRP) according to the scheme in Supporting Information Figure S2.[39] The details of polymer synthesis may be found in the supporting information. After polymerization, the synthesis medium was transferred into a Spectra/Por$^{(R)}$ molecular porous membrane tubing having a molecular weight cut off of 3500 Da. The solution was dialyzed for 2 weeks at room temperature while replacing the Millipore water every day. The resulting solution was then transferred to a

dialysis tubing having a molecular cut off of 12,000–14,000 Da. and dialyzed against Millipore water for an additional 2 weeks at 40°C. The sample was centrifuged, and the polymer solution was frozen and the water sublimated at low pressure in the freeze-drying process to yield a white powder.

Characterization

^{1}H-NMR analyses on the polymer samples for synthesis characterization were conducted with a Bruker 600 MHz high resolution Ultra Shield™ spectrometer. NMR experiments were performed on PEG_{110}-Br, Me_6TREN, and PEG-*b*-PNIPAM polymers to confirm the successful synthesis. The spectra of PEG_{110}-Br, Me_6TREN, and PEG_{110}-*b*-$PNIPAM_{243}$ are shown in Supporting Information Figure S3–S5. The ^{1}H-NMR spectra revealed that the hydroxyl group of PEG_{110}-OH was fully esterified and the PEG-*b*-PNIPAM polymers were synthesized successfully. The molecular weight of the polymer was calculated using the integration of the PEG peaks to the PNIPAM peaks (1.00 and 3.55 ppm, respectively). The molecular weight of PEG_{110}-*b*-$PNIPAM_{243}$ was determined to be 32,500 g/mol, which corresponded to ~90% conversion of the NIPAM monomer. In addition, PEG_{110}-*b*-$PNIPAM_{186}$ and PEG_{110}-*b*-$PNIPAM_{223}$ were also synthesized and characterized by NMR.

Gel Permeation Chromatography (GPC) system was used to determine the distribution and PDI of polymer samples. The GPC system consisted of a Millipore pump, a Wyatt MiniDawn light scattering detector and a Millipore Waters 410 differential refractometer. The data was analyzed using the Advanced Sysinfo Tool and Reporting Assistant for Windows software. The GPC traces of the PEG_{110}-OH starting material and the final PEG_{110}-*b*-$PNIPAM_{243}$ product are shown in Supporting Information Figure S6. The final polymer had a lower retention volume than that of the starting material, and this was evidence of polymerization since higher weight polymers elute faster through the column. Both graphs showed a monomodal distribution that confirmed that only one size of polymer existed in both samples. The GPC showed a PDI of 1.2 for the PEG_{110}-OH and 1.6 for PEG_{110}-*b*-$PNIPAM_{243}$.

Measurements

Sample Preparation. The polymer solutions were prepared individually by dissolving PEG-*b*-PNIPAM in purified Millipore water. For the study of PEG_{110}-*b*-$PNIPAM_{243}$/α-CD complexes, an appropriate amount of α-CD (98%; Sigma Aldrich) was added to PEG_{110}-*b*-$PNIPAM_{243}$ solutions. The resulting solution was stirred and agitated ultrasonically to promote dissolution. The samples were then stored in the refrigerator overnight prior to use to allow time for the self-assembly process to reach an equilibrium. For light scattering measurements, the samples were passed through a 0.45 μm Millipore mixed cellulose ester (HAWP) membrane filter that had been preflushed with purified water. The samples were centrifuged for 30–60 min at a speed of 4500 rpm immediately before use.

Surface Tension. Surface tension data was obtained using a DataPhysics dynamic tensiometer equipped with a Wilhelmy plate, based on the increasing concentration method. For the first experiment, 0.1 wt % PEG_{110}-*b*-$PNIPAM_{243}$ was titrated into 50 mL of water at 40°C. For the second experiment, 0.1 wt % PEG_{110}-*b*-$PNIPAM_{243}$ in 0.009826 M α-CD was titrated into 50 mL of water at 25°C. The surface tension data was plotted to gain information on the critical micelle concentration (CMC) and head group size of the systems.

By plotting the surface tension against the concentration (γ vs. ln C), the CMC can be determined by locating the intercept of the two linear regions of the plot. The Gibb's equation (eq. 1) relates the slope of the linear region of the γ vs. ln C plot to the surface concentration (Γ).

$$\Gamma = \frac{-1}{RT}\left(\frac{\Delta\gamma}{\Delta \ln C}\right) \quad (1)$$

where Γ is the surface concentration, R is the gas constant, T is the temperature, γ is the surface tension, and C is the concentration of the surfactant. Using Avogadro's number, Γ may be converted to the head group area (a_o).

Isothermal Titration Calorimetry. Calorimetric titration measurements were carried out using a Microcal Isothermal Titration Calorimeter (ITC) with a 1.4-mL sample cell in an adiabatic shield. The stirring rate was set to 400 rpm and the time between injections was set to 250 s. The data was recorded automatically, and the Microcal ORIGIN for ITC program was used to integrate and generate differential enthalpy curves. The data was analyzed using a sequential binding site model, and the Marquardt minimization routine was used to obtain the values of the fitting parameters.

For the ITC, a PEG_{110}-*b*-$PNIPAM_{243}$ solution and α-CD solution was prepared at 0.1 and 2 wt %, respectively. The reference cell was filled with water. The α-CD was titrated into the polymer solution at both 25.0 ± 0.02°C and 40.0 ± 0.02°C.

Light Scattering. The microstructures of the samples were examined by a Brookhaven Laser Light Scattering system. The system has a BI200SMv2 goniometer, TurboCorr Coorelator and a MiniL-20 636 nm laser. dn/dc measurements were conducted using a Brookhaven BI-DNDC differential refractometer.

For dynamic light scattering (DLS), the temporal intensity fluctuations for a sample were measured at 60, 75, 90, 105, 120, 135, and 150°. The data from the detector was transferred to the GENDIST (General Distribution) software package to perform the inverse Laplace transform. GENDIST uses the REPES (Regularized Positive Exponential Sum) algorithm.[41] The probability of reject was set to 0.5. A linear relationship in the plot of Γ vs. q^2 was used to confirm that the scattering is attributed to translation diffusion. The average diffusion coefficient of the particles was obtained from the slope of the Γ vs. q^2 plot. Using the Stokes-Einstein equation, the R_h was calculated.

For static light scattering (SLS) the time-averaged intensities of scattered light for a sample was measured at angles ranging from 50° to 150° in 10° intervals. Using the partial Zimm equation, the R_g may be determined by the slope and intercept of $1/I_{ex}(q)$ vs. q^2 plot.[42] The ratio of R_g and R_h values is commonly used to indicate the morphology of microstructure of the aggregates.[43] Table I summarizes the typical R_g/R_h ratios for a variety of structural conformations.

Differential Scanning Calorimetry. The Differential Scanning Calorimeter (DSC) used to conduct experiments contained a 0.5 mL sample cell held in an adiabatic shield. Data on the enthalpy change due to a system's phase transition was evaluated using the Origin software. DSC samples were prepared by adding the

Table I. Conformational Information from R_g/R_h Ratios

R_g/R_h	Structure
<0.6	Core-shell
~0.774	Hard Sphere
~1	Vesicle
~1.5	Gaussian Chain
>2	Long Rod

appropriate amount of α-CD to 0.1 wt % PEG-*b*-PNIPAM samples. DSC measurements were conducted from 10 to 90°C in both upscan and down scan directions.

RESULTS AND DISCUSSION

Visual Observations

PEG_{110}-*b*-$PNIPAM_{243}$ solutions of 0.1 wt % were clear at room temperature, which suggested that both segments were hydrophilic and the polymer existed as free chains. Increasing the temperature above the LCST caused the solution to become opaque; however, the particles did not agglomerate to form precipitates like PNIPAM homopolymers, which suggested that micellization of unimeric chains had occurred. The PNIPAM segments most likely formed the core and the PEG segments stabilized the particles by forming the surrounding corona. The addition of α-CD to the PEG_{110}-*b*-$PNIPAM_{243}$ solution did not change the visual characteristics of the solution below the LCST. Supramolecular structures formed from the micellization of polymer ICs have been found to produce clear solutions.[38,44] Above the LCST, the solution became stable and opaque (Figure 1).

Surface Tension

CMC is an important property used to characterize the self-assembly property of aqueous block copolymer solutions. Surface tension measurements of 0.1 wt % PEG_{110}-*b*-$PNIPAM_{243}$ at 40°C and of 0.1 wt % PEG_{110}-*b*-$PNIPAM_{243}$ in 0.00695 M α-CD at 25°C are shown in the Supporting Information Figure S7, and their CMC values were 0.00058 g/L and 0.0012 g/L, respectively. The CMC of PEG_{110}-*b*-$PNIPAM_{243}$ was comparatively lower than that of PEG_{110}-*b*-$PNIPAM_{243}$/α-CD, which indicated that the hydrophobic PNIPAM segments were less soluble than the PEG/α-CD complexes.[45] The surface excess concentration was used to calculate the head group area of the molecules. For PEG_{110}-*b*-$PNIPAM_{243}$ and for PEG_{110}-*b*-$PNIPAM_{243}$/α-CD, the areas were 29.2 $Å^2$ and 14.7 $Å^2$, respectively. Smaller polymer aggregates partition to the air-water interface with a higher packing efficiency that individual polymer chains.[46] The diameter of α-CD is approximately 4.5 Å.[47] The area of a single α-CD corresponded closely with the surface area/molecule of PEG_{110}-*b*-$PNIPAM_{243}$/α-CD. This suggested that the α-CD included column structures stand perpendicular to the water surface.

Isothermal Titration Calorimetry

ITC was used to characterize the thermodynamics of binding and the self-assembly of the polymeric systems. Calorimetric measurements were conducted as α-CD was titrated into the PEG_{110}-*b*-$PNIPAM_{243}$ solution at both 25.00 ± 0.02°C and 40.00 ± 0.02°C. In both cases, the raw data resulting from the titration isotherms for α-CD into water were subtracted from the titration isotherms of α-CD into PEG_{110}-*b*-$PNIPAM_{243}$ solutions and integrated to yield the Δ*H* binding curve. Figure 2(a, b) show the titration of 2 wt % α-CD into 0.1 wt % PEG_{110}-*b*-$PNIPAM_{243}$ at 25°C. A clear binding curve was observed and, assuming two EG units per CD molecule,[33,48–51] near-complete coverage was exhibited. The initial data points did not fit in a traditional CD-PEG binding curve. At concentrations nearing saturation, CD in solution form large aggregated systems of around 2700 nm.[52] In addition, PEG is known to aggregate into three dimensional network structures.[53] As CD was titrated, the hydrogen bonds and hydrophobic interactions responsible for these structures must first be disrupted before CD threading can occur. Further evidence of the existence of PEG structures was revealed by laser light scattering and this will be discussed later. The initial 10 data points were omitted because they are related to the disruption of hydrogen bonds, and a two-site sequential binding model was used to fit the calorimetric data of binding. The results are displayed in Table II.

The fitting of the three site model indicated three sequential events occurring as α-CD was added. Since the Δ*H* values are the sum of several interactions, including α-CD/α-CD interactions, α-CD/polymer interactions, α-CD and chain hydration, and hydrocarbon interactions, at this time it is difficult to quantitatively determine the contributions from each interaction. Hydrophobic interaction is characterized by small positive Δ*H* and Δ*S*, and van der Waals interaction is characterized by a negative Δ*H*.[54] The first event showed a negative Δ*H* value and a positive Δ*S* value. The positive Δ*H* value is indicative of van der Waals interactions. Therefore, it was believed that the first event was a result of α-CD-polymer binding through hydrogen bonding. The second event resulted in positive Δ*H* and Δ*S* values, which indicated that the event was caused by hydrophobic interactions. Yuan and Shuai[37] noted that threading of α-CD molecules onto the PPG segment consumed most of the available hydroxyl groups causing the α-CD molecules to become

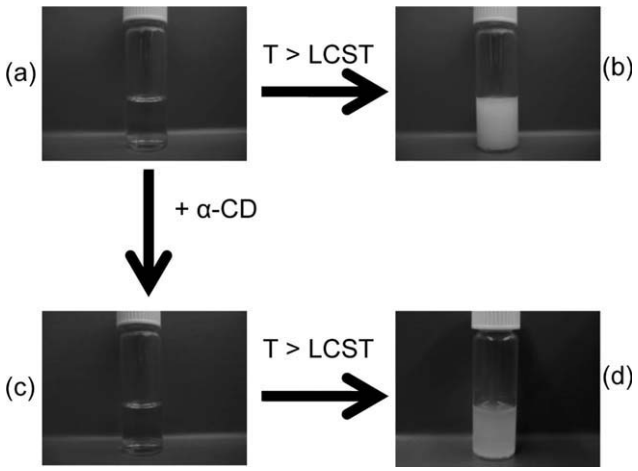

Figure 1. Photographs of PEG_{110}-*b*-$PNIPAM_{243}$ solutions at various conditions: (a) 25°C, (b) 40°C, (c) 25°C with α-CD, and (d) 40°C with α-CD.

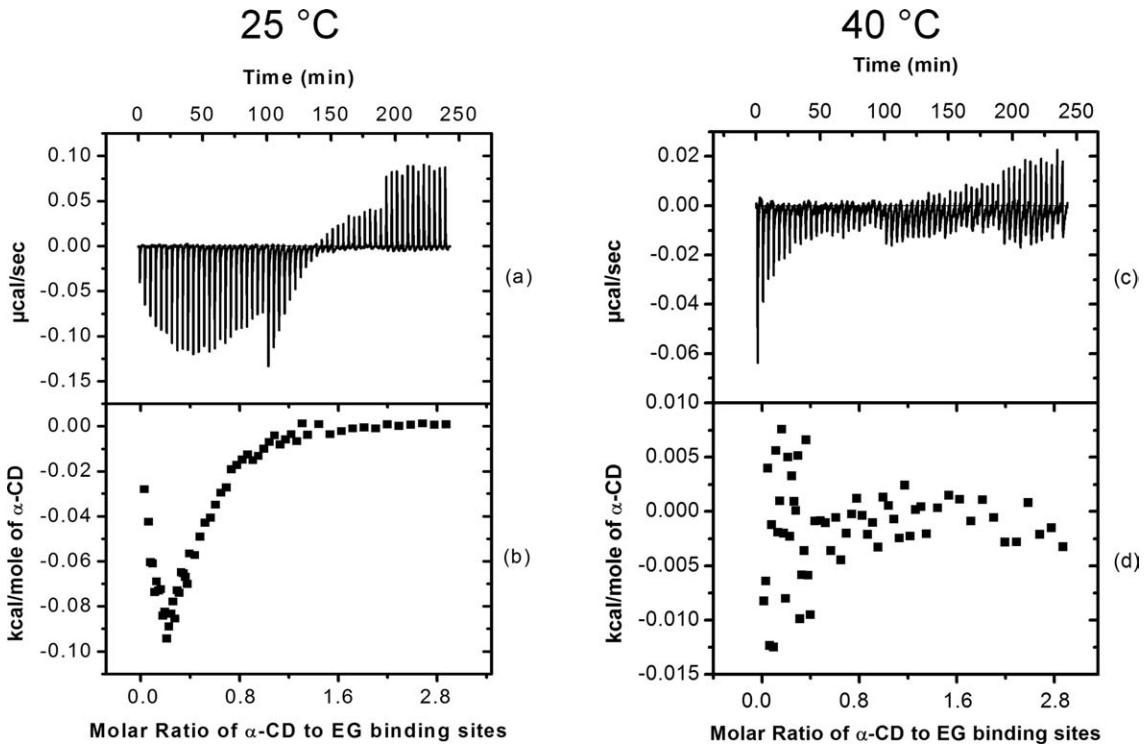

Figure 2. Calorimetric titration of 2 wt % α-CD into 0.1 wt % PEG_{110}-*b*-$PNIPAM_{243}$ solution. (a) Thermogram showing the cell feedback power versus time at 25°C. (b) Differential enthalpy versus molar ratio of α-CD to EO binding sites at 25°C. (c) Thermogram showing the cell feedback power versus time at 40°C. (d) Differential enthalpy versus molar ratio of α-CD to EO binding sites at 40°C.

hydrophobic. It was then possible for the polymer complex to form aggregated structures.[37] Therefore, the second event was believed to result from the supermolecular aggregation of chains into a micellar structure. The third event was a result of van der Waals interactions and was believed to contribute to the stabilization of the micelles after their formation.

Figure 2(c, d) show the titration of 0.2 wt % α-CD into 0.1 wt % PEG_{110}-*b*-$PNIPAM_{243}$ at 40°C. In contrast to the titration at 25°C [Figure 2(b)], Figure 2(d) shows no binding interactions. The data points were concentrated around 0.00 kcal/mole of α-CD. At 40°C, since no α-CD threading was shown by the ITC results, it was believed that the polymer system would exhibit properties similar to those of the blank polymer (without α-CD); the PEG_{110}-*b*-$PNIPAM_{243}$ formed micelles with PNIPAM cores. α-CD is known to have difficulty threading at elevated temperatures.[44]

Light Scattering

The refractive index increment measurement was performed on the PEG_{110}-*b*-$PNIPAM_{243}$ sample and the dn/dc was found to be $1.642 \times 10^{-1} \pm 2.6 \times 10^{-3}$ mL/g. Count rate measurements were performed for 0.1 wt % PEG_{110}-*b*-$PNIPAM_{243}$ (filled circles) and 0.0025 wt % PEG_{110}-*b*-$PNIPAM_{243}$ in 0.000174 M α-CD (unfilled circles) over a variety of temperatures, and their results are shown in Figure 3. Below the LCST, PEG_{110}-*b*-$PNIPAM_{243}$ chains were hydrophilic, and they existed as unimeric chains as indicated by the low count rate. Comparing the results of PEG_{110}-*b*-$PNIPAM_{243}$ and PEG_{110}-*b*-$PNIPAM_{243}$/α-CD, the lower count rates for the PEG_{110}-*b*-$PNIPAM_{243}$/α-CD below the LCST are related to the much lower concentration used in the study. Above the LCST, micelles were formed, and this corresponded to a large jump in the count rates. Similarly, for the PEG_{110}-*b*-$PNIPAM_{243}$/α-CD sample, supramolecular structures formed at low temperature; but, at low concentrations, these structures did not scatter light intensely either. Above the LCST, a sudden increase in count rate occurred, which corresponded to aggregation in the system.

Because of large scattering of PEG_{110}-*b*-$PNIPAM_{243}$/α-CD structures, the count rate experiment for PEG_{110}-*b*-$PNIPAM_{243}$/α-CD was performed at lower concentration, laser strength, and pin hole size. The 0.1 wt % PEG-*b*-PNIPAM started at 45.1 kcps

Table II. Calorimetric Data from Three-Site Sequential Binding Model for PEG110-b-PNIPAM243/α-CD

	1	2	3
K (L/mol)	$9.0 \times 10^4 \pm 1.3 \times 10^4$	$1.0 \times 10^5 \pm 2.1 \times 10^4$	$1.11 \times 10^5 \pm 3.0 \times 10^4$
Δ*H* (cal/mol)	−158.5 ± 7.7	549.4 ± 41.0	−757.7 ± 95.6
Δ*S* (cal/mole/K)	22.1	24.8	20.5

Applied Polymer SCIENCE

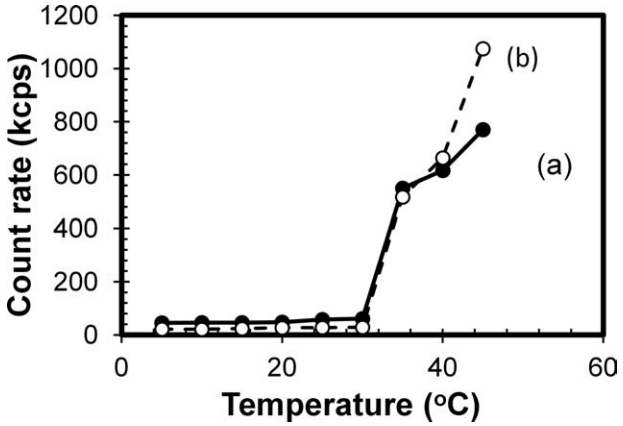

Figure 3. Plot of count rate versus temperature for (a) 0.1 wt % PEG_{110}-*b*-$PNIPAM_{243}$ and (b) 0.0025 wt % PEG_{110}-*b*-$PNIPAM_{243}$ in 0.174 m*M* α-CD.

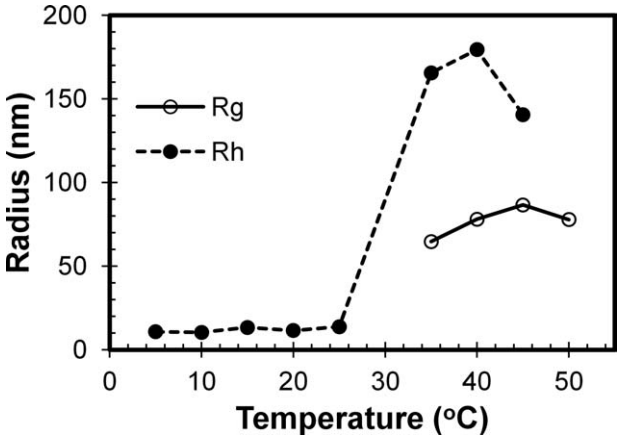

Figure 5. Effect of temperature on the R_g and R_h of PEG_{110}-*b*-$PNIPAM_{243}$. The samples were measured at 0.1 wt % below the LCST and 0.005 wt % above the LCST.

below the LCST and increased to 770.6 kcps above the LCST, and the 0.0025 wt % PEG_{110}-*b*-$PNIPAM_{243}$/α-CD increased from 21.8 below the LCST to 1074.5 kcps above the LCST. Although the count rates were not directly comparable, this difference in count rate increase indicated that the change of the PEG_{110}-*b*-$PNIPAM_{243}$/α-CD over temperature was greater than that of PEG_{110}-*b*-$PNIPAM_{243}$ system.

DLS and SLS measurements were conducted on PEG_{110}-*b*-$PNIPAM_{243}$ and PEG_{110}-*b*-$PNIPAM_{243}$/α-CD samples. Below the LCST, the decay time distributions were seen to possess two decay modes. PEG is known to be soluble in water at room temperature due to the formation of hydrogen bonds between the ether groups and water. However, PEG aggregation is commonly observed and reported.[53,55,56] There are two explanations for the aggregation of PEG into three-dimensional structures. The first is the interaction between the hydrophobic -(CH_2CH_2)- and end groups, and the second are the hydrogen bonded water molecules acting as cross-linkers for the PEG clusters in solution. In the study by Dai and Tam,[53] they found

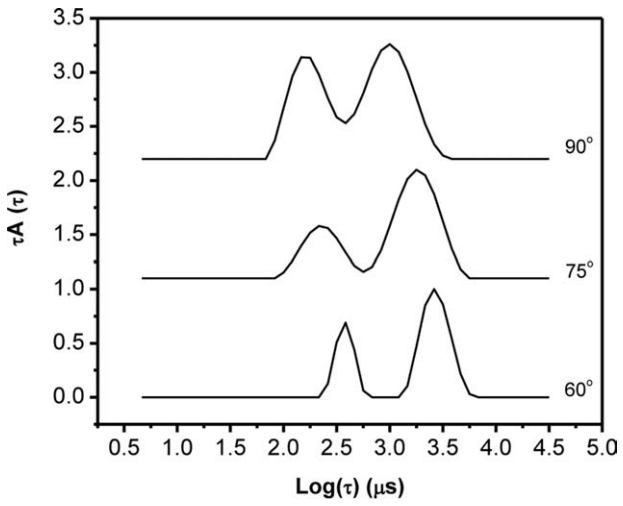

Figure 4. Decay distribution functions for 0.1 wt % PEG_{110}-*b*-$PNIPAM_{243}$ at 20°C.

that samples of 0.1 wt % PEG (300 K) in water showed two angular dependent decay modes with R_h values of 26 and 275 nm with diffusion coefficients of 9.4×10^{-12} m^2/s and 8.9×10^{-13} m^2/s, respectively. It was determined that the fast decay mode with the small R_h values corresponded to unimeric PEG chains and the slow decay mode with the larger R_h values corresponded to the aggregation of PEG clusters. Figure 4 shows the time distribution for 0.1 wt % PEG_{110}-*b*-$PNIPAM_{243}$ at 20°C. Both decay modes were q^2 dependent, and, therefore, the two peaks were due to two types of particles in solution. The R_h values were determined to be 11.6 nm and 73.4 nm. The diffusion constants were determined to be 1.9×10^{-11} m^2/s and 2.9×10^{-12} m^2/s. Since the molecular weight of PEG_{110}-*b*-$PNIPAM_{243}$ was much lower than that of the PEG used in an earlier study,[53] it is understandable that the R_h values determined were also lower. The 11.6 nm particles with the faster diffusion coefficient were attributed to unimeric PEG_{110}-*b*-$PNIPAM_{243}$ chains, and the 73.4 nm particles with the slower diffusion coefficient were attributed to the aggregated PEG clusters. It was noted that filtration removes the aggregated particles; however, measurements must be taken immediately. This was not possible for this set of experiment due to the centrifugation in the sample preparation method, the temperature equilibration before each measurement, and the number of measurements needed for each sample. Above the LCST, only one decay mode was present.

The resulting R_h and R_g values versus temperature for PEG_{110}-*b*-$PNIPAM_{243}$ and PEG_{110}-*b*-$PNIPAM_{243}$/α-CD samples are shown in Figures 5 and 6, respectively. For PEG_{110}-*b*-$PNIPAM_{243}$ (Figure 6), the R_h values below the LCST were small, averaging 11.6 nm, which corresponded to free polymeric chains in solution. At the LCST, the R_h increased to over 145 nm, which clearly indicated a change in the morphology.[53] Data for R_g values were not attainable below the LCST, and this was confirmation of free chains in solution as free polymers do not display angular dependence. Figure 7 displays the calculated R_g/R_h values versus temperature for PEG_{110}-*b*-$PNIPAM_{243}$. Above the LCST, the R_g/R_h values clearly corresponded to core-shell micelle structures,[36] which agreed with previous reported studies.[23–26]

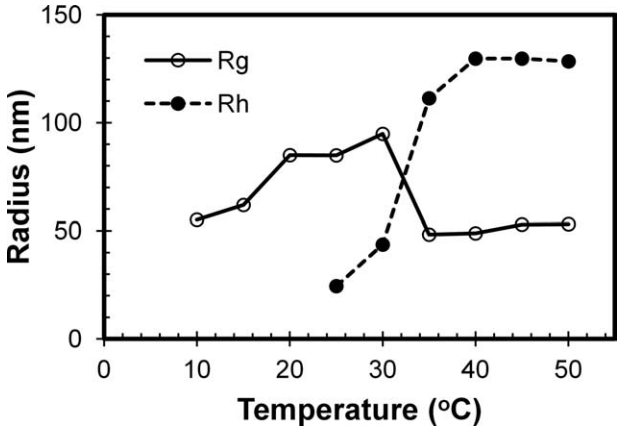

Figure 6. Effect of temperature on the R_g and R_h of PEG_{110}-*b*-$PNIPAM_{243}$/α-CD. The samples were measured at 0.1 wt % PEG_{110}-*b*-$PNIPAM_{243}$ and 6.95 mM α-CD below the LCST and 0.005 wt % PEG_{110}-*b*-$PNIPAM_{243}$ and 0.6475 mM α-CD above the LCST.

For PEG_{110}-*b*-$PNIPAM_{243}$/α-CD (Figure 6), the R_h values below the LCST were significantly larger than those of PEG_{110}-*b*-$PNIPAM_{243}$ (Figure 5), and these values indicated that the polymer chains were not in their unimeric form. Above the LCST, R_h increased, showing a change in the morphology. R_g values for PEG_{110}-*b*-$PNIPAM_{243}$/α-CD, below the LCST, increased with increasing temperature. However, it should be noted that due to the condensation on the vat and the sample tube, data below 20°C or 25°C may be unreliable. Above the LCST, there was a sharp decrease in R_g values, which indicated possible morphological change. The R_g/R_h values versus temperature for PEG_{110}-*b*-$PNIPAM_{243}$/α-CD are displayed in graphical form in Figure 7. Below the LCST, the data showed a rod-like configuration, and, above the LCST, the values corresponded to

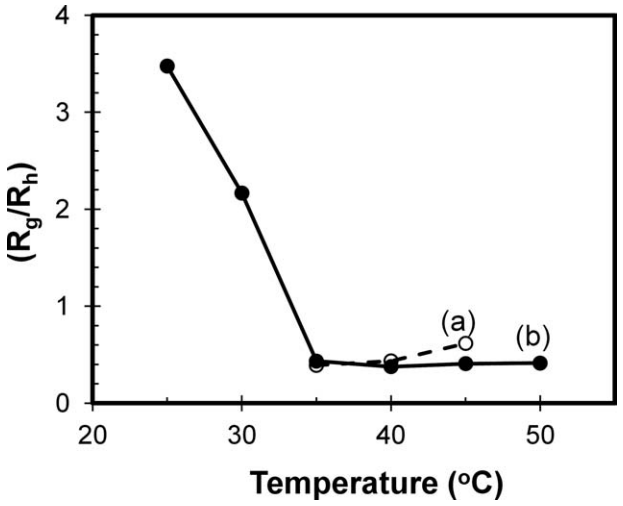

Figure 7. Effect of temperature on the conformational ratios for (a) PEG_{110}-*b*-$PNIPAM_{243}$ and (b) PEG_{110}-*b*-$PNIPAM_{243}$/α-CD. Below the LCST, the samples were measured at (a) 0.1 wt % PEG_{110}-*b*-$PNIPAM_{243}$ and (b) 0.1 wt % PEG_{110}-*b*-$PNIPAM_{243}$ with 6.95 mM α-CD. Above the LCST, the samples were measured at (a) 0.005 wt % PEG_{110}-*b*-$PNIPAM_{243}$ and (b) 0.005 wt % PEG_{110}-*b*-$PNIPAM_{243}$ with 0.3475 mM α-CD.

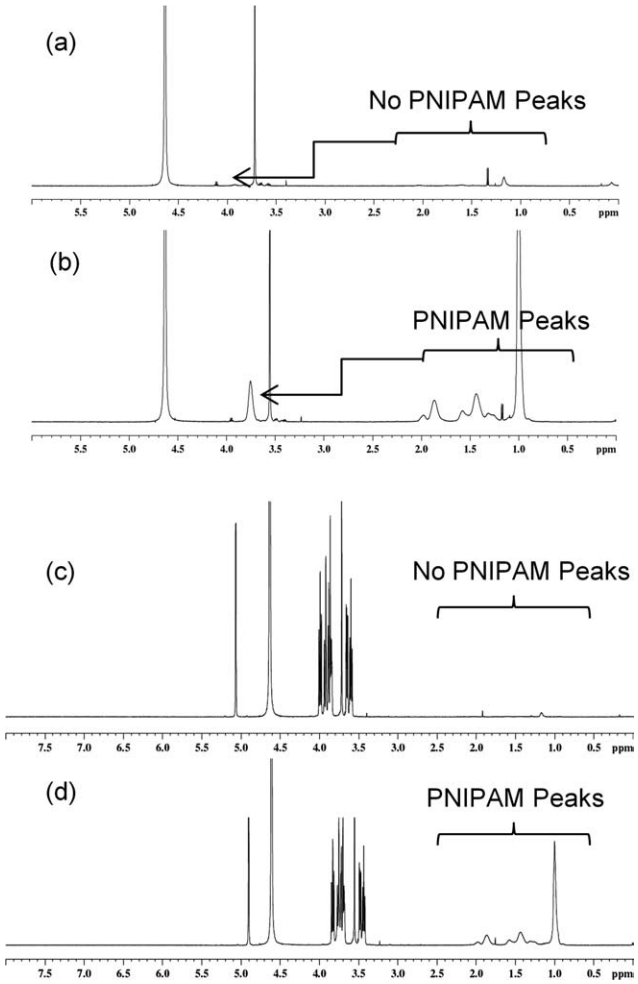

Figure 8. NMR spectra of (a) PEG_{110}-*b*-$PNIPAM_{243}$ at 40°C, (b) PEG_{110}-*b*-$PNIPAM_{243}$ at 25°C, (c) PEG_{110}-*b*-$PNIPAM_{243}$/α-CD at 40°C, and (d) PEG_{110}-*b*-$PNIPAM_{243}$/α-CD at 25°C in D_2O.

spherical micelles.[36] The R_g/R_h values of these spherical micelles were similar to PEG_{110}-*b*-$PNIPAM_{243}$. This confirmed that the α-CD dethreaded from the polymeric chain, and micelles consisting of PNIPAM core and PEG corona were formed. The alternative hypothesis of micelles composed of PNIPAM core and PEG/α-CD corona was incorrect because the R_g value of the system would be larger than that of PEG_{110}-*b*-$PNIPAM_{243}$ (due to increased weight in the corona) and the R_g/R_h values would be larger. Supporting Information Figure S21 displays a schematic to illustrate this observation.

DLS measurements of the samples were then performed using a vertical-horizontal polarizer. Weak correlations were found for the system at 25°C, 90° angle, and at high concentration only. Insufficient data could be collected for proper analysis of the rod dimensions. However, the weak correlation indicated that the rod was flexible.

Temperature Analysis with NMR

Figure 8 shows the ^{1}H-NMR spectra of PEG_{110}-*b*-$PNIPAM_{243}$ and PEG_{110}-*b*-$PNIPAM_{243}$/α-CD at 25°C and 40°C. Dai et al. used ^{1}H-NMR to study the morphology of reversible block

Table III. Calorimetric Data for Phase Transitions of PEG-*b*-PNIPAM with Various NIPAM Block Lengths

Polymer	T_m (°C)	ΔH (cal/mol)	ΔS (cal/mol/°C)
PEG_{110}-*b*-$PNIPAM_{186}$	36.6	2.73×10^5	6.99×10^3
PEG_{110}-*b*-$PNIPAM_{223}$	34.9	3.02×10^5	8.70×10^3
PEG_{110}-*b*-$PNIPAM_{243}$	34.5	4.41×10^5	1.25×10^4

copolymer micelles because peaks corresponding to the solvated blocks were clearly detected and the blocks were not observed in the NMR spectra corresponded to the condensed core.[57] For the PEG_{110}-*b*-$PNIPAM_{243}$ block copolymer, at 25°C [Figure 8(b)], the signals at 1–2 ppm and 3.75 ppm corresponded to the PNIPAM segments. These peaks were clearly detected in the spectra and were indicative that the PNIPAM blocks were solvated in the solvent (D_2O). At 40°C [Figure 8(a)], the PNIPAM peaks disappeared, and the PEG peaks were observed and they were attributed to the temperature increase. This information revealed that at 25°C, the polymer existed as free chains, and core-shell micelles composing of a PNIPAM core were produced at 40°C. For the PEG_{110}-*b*-$PNIPAM_{243}$/α-CD sample at 25°C [Figure 8(d)], the signals at 1–2 ppm and 3.75 ppm corresponded to the PNIPAM segments. These peaks were clearly detected in the spectrum and were indicative that the PNIPAM block was solvated in the solvent (D_2O). The CD peaks were seen at this temperature due to an excess of CD in solution. At 40°C [Figure 8(c)], the PNIPAM peaks disappeared, and the PEG and CD peaks were observed to be more dominant. This information confirmed the micellar structure with PEG/α-CD condensed phase at 25°C and that the PNIPAM dispersed phase reversed to a core-shell micelle of PNIPAM core at 40°C.

Differential Scanning Calorimetry

For PEG-*b*-PNIPAM, DSC can provide information on the enthalpy (ΔH), change in heat capacity (C_p), and the LCST of the phase transition. The C_p data attained was normalized, and the baseline was subtracted before determining the ΔH, ΔS, and ΔG values of the transition. Table III summarizes the transition data for three PEG-*b*-PNIPAM polymers with varying PNIPAM block lengths. T_m is the transition temperature. Table IV shows the results of PEG_{110}-*b*-$PNIPAM_{243}$/α-CD where T_m is the transition temperature, and T^* and T^{**} are the temperatures at which the phase transition begins and ends (i.e., the temperature at which the C_p data deviates from and merges with the baseline—Supporting Information Figure S22).

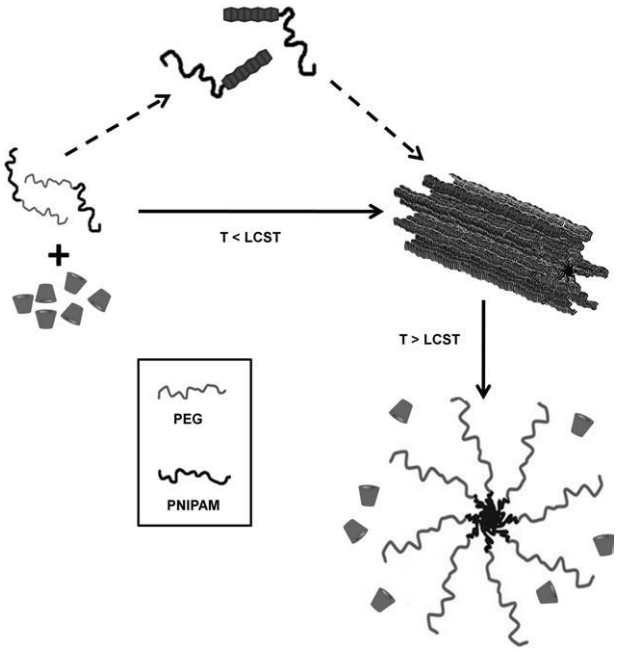

Figure 9. Schematic representation of the morphology of PEG_{110}-*b*-$PNIPAM_{243}$/α-CD.

The T_m values were within a few degrees of the expected T_m for PNIPAM homopolymers, and the ΔH values were in reasonable range of the values obtained by Tang et al. in their PNIPAM homopolymer studies.[58] The LCST of PEG-*b*-PNIPAM was found to be higher than that of PNIPAM homopolymer. Ding and Zhang[59] studied the effect of adding PEG homopolymers on the phase transition of PNIPAM homopolymers, and they found that at low PEG concentrations, as in this study, the T_m increased and the ΔH decreased due to PEG suppressing the interchain aggregation of PNIPAM chains. Similarly, in this study, the hydrophilicity of the PEG segment made it more difficult for the polymer to phase separate. As the PNIPAM block length increased, the transition temperature decreased to a value closer to that of PNIPAM homopolymer. With increasing NIPAM block length, the change in enthalpy and entropy increased which indicated more compact aggregates and greater conformational change.[59] In the study of PEG_{110}-*b*-$PNIPAM_{243}$/α-CD, increase in the mole ratio of α-CD to polymer was found

Table IV. Calorimetric Data for Phase Transitions of PEG_{110}-*b*-$PNIPAM_{243}$/α-CD

Mole ratio of α-CD to EG binding sites	T_m (°C)	ΔH (cal/mol)	ΔS (cal/mol/°C)	ΔG at T^* (cal/mol)	ΔG at T^{**} (cal/mol)
0	34.47	4.41×10^5	1.25×10^4	1.37×10^5	-8.82×10^4
0.53	34.50	4.18×10^5	1.18×10^4	1.31×10^5	-1.18×10^5
0.64	34.51	3.97×10^5	1.13×10^4	1.30×10^5	-9.12×10^4
2.96	34.58	3.45×10^5	9.65×10^3	9.41×10^4	-9.55×10^4
5.93	34.62	3.18×10^5	8.75×10^3	3.24×10^4	-1.18×10^5
21.26	35.07	2.80×10^5	7.71×10^3	2.07×10^4	-8.45×10^4

to cause the T_m to increase and the ΔH and ΔS values to decrease, which indicated that the transitions resulted in lesser conformational change and looser aggregations.[59] The phase transition became increasingly more difficult as CD was added. This was thought to be due to both the threading of the CD onto the EG segment and the hydrogen bonding of the CD to the polymer.

At 25°C, CD was shown to bind with PEG_{110}-*b*-$PNIPAM_{243}$, but not at 40°C. This indicated that the hydrophobicity of PNIPAM at 40°C deters the threading of CD. Below the LCST, the PEG_{110}-*b*-$PNIPAM_{243}$ samples showed no angular dependence with small R_h values, and these results were indicative of solvated free chains. PEG_{110}-*b*-$PNIPAM_{243}$ samples above the LCST showed larger R_g values and smaller R_g/R_h values than that of PEG_{110}-*b*-$PNIPAM_{243}$/α-CD. This data was evidence that the polymer chains formed a micellar structure with solvated chains. For PEG_{110}-*b*-$PNIPAM_{243}$/α-CD, samples below the LCST displayed angular dependence and larger R_g/R_h values than those of PEG_{110}-*b*-$PNIPAM_{243}$. Along with the polarized DLS study, the data corresponded to flexible rod morphology. Above the LCST, it was believed that the CD dethreaded from PEG segment, and core-shell micelles with a PNIPAM core and PEG corona reformed. Above the LCST, the PNIPAM ^{1}H-NMR peaks disappeared, which indicated structure containing a PNIPAM core and PEG/α-CD desolvated chains. In summary, at 25°C, CD threaded onto the PEG section of PEG_{110}-*b*-$PNIPAM_{243}$ to form a rod-shaped micelle. At 40°C, the CDs dethreaded from the polymer and a core-shell micelle of PNIPAM core and PEO corona was formed. A schematic summary of morphology is shown in Figure 9. By comparing the thermodynamic parameters of the phase transitions for samples at multiple CD concentrations, it was observed that the addition of CD hindered the ability of the system to phase separate.

CONCLUSIONS

In this study, PEG-*b*-PNIPAM polymer systems were investigated to determine the morphological changes exhibited as a result of cyclodextrin complexation and temperature phase transition. Using techniques, such as surface tensiometry, ITC, LLS, and DSC, the micellization characteristics of the PEG-*b*-PNIPAM/α-CD systems were elucidated. Threading of α-CD onto PEG segments of PEG-*b*-PNIPAM induced the self-assembly of the block copolymer into cylindrical micelles which, above the LCST, transformed into a spherical micelles after releasing the CDs back into solution. This system, with the biocompatible PEO shell, may prove useful in drug delivery applications as it has the ability to release CD conjugated drug molecules at body temperature. The ability to control the architecture of a polymer system through complexation with CD and external stimuli allows the systems to be potentially incorporated into sophisticated applications. Significant opportunities exist in combining a variety of control strategies to tailor the morphology of nanostructures to suit a specific need, and it is anticipated that the topic of multi-stimuli responsive inclusion complex systems will continue to be an active area of research.

ACKNOWLEDGMENTS

The authors would like to acknowledge the financial support provided by NSERC, CFI, Ontario Government, and the Waterloo Institute for Nanotechnology to facilitate the current research on block copolymers.

REFERENCES

1. Hoeben, F. J. M.; Jonkheijm, P.; Meijer, E. W.; Schenning, A. *Chem. Rev.* **2005,** 1491.
2. Yagai, S.; Kitamura, A. *Chem. Soc. Rev.* **2008,** *37*, 1520.
3. Brunsveld, L.; Folmer, B. J. B.; Meijer, E. W.; Sijbesma, R. P. *Chem. Rev.* **2001,** *101*, 4071.
4. Vriezema, D. M.; Aragones, M. C.; Elemans, J.; Cornelissen, J.; Rowan, A. E.; Nolte, R. J. *M. Chem. Rev.* **2005,** *105*, 1445.
5. Dai, S.; Ravi, P.; Tam, K. C. *Soft Matter* **2008,** *4*, 435.
6. Xiong, X. Y.; Tam, K. C.; Gan, L. H. *J. Control. Release* **2005,** *103*, 73.
7. Farokhzad, O. C.; Langer, R. *Adv. Drug Deliv. Rev.* **2006,** *58*, 1456.
8. Betancourt, T.; Brannon-Peppas, L. *Int. J. Nanomed.* **2006,** *1*, 483.
9. Brannon-Peppas, L.; Blanchette, J. O. *Adv. Drug Deliv. Rev.* **2004,** *56*, 1649.
10. Puvvada, S.; Blankschtein, D. J. *Chem. Phys.* **1990,** *92*, 3710.
11. Nishiyama, N.; Kataoka, K. *Pharmacol. Therapeutics* **2006,** *112*, 630.
12. Peppas, N. A.; Hilt, J. Z.; Khademhosseini, A.; Langer, R. *Adv. Mater.* **2006,** *18*, 1345.
13. Chiappetta, D. A.; Sosnik, A. *Eur. J. Pharmaceutics Biopharma.* **2007,** *66*, 303.
14. Xiong, X. Y.; Tam, K. C.; Gan, L. H. *J. Nanosci. Nanotechnol.* **2006,** *6*, 2638.
15. Nakashima, K.; Bahadur, P. *Adv. Colloid Interface Sci.* **2006,** *123*, 75.
16. Chen, X. Y.; Gao, B.; Kops, J.; Batsberg, W. *Polymer* **1998,** *39*, 911.
17. Yu, K.; Eisenberg, A. *Macromolecules* **1998,** *31*, 3509.
18. Dai, S.; Ravi, P.; Leong, C. Y.; Tam, K. C.; Gan, L. H. *Langmuir* **2004,** *20*, 1597.
19. Alexandridis, P.; Hatton, T. A. *Colloids Surfaces a-Physicochem. Eng. Aspects* **1995,** *96*, 1.
20. Schild, H. G. *Prog. Polym. Sci.* **1992,** *17*, 163.
21. Afrassiabi, A.; Hoffman, A. S.; Cadwell, L. A. *J. Membr. Sci.* **1987,** *33*, 191.
22. Arotcarena, M.; Heise, B.; Ishaya, S.; Laschewsky, A. J. *Am. Chem. Soc.* **2002,** *124*, 3787.
23. Virtanen, J.; Holappa, S.; Lemmetyinen, H.; Tenhu, H. *Macromolecules* **2002,** *35*, 4763.
24. Motokawa, R.; Nakahira, T.; Annak, M.; Hashimoto, T.; Koizumi, S. *Polymer 45*, 9019.

25. Topp, M. D. C.; Dijkstra, P. J.; Talsma, H.; Feijen, J. *Macromolecules* **1997,** *30*, 8518.
26. Zhang, W. Q.; Shi, L. Q.; Wu, K.; An, Y. G. *Macromolecules* **2005,** *38*, 5743.
27. Qin, S. H.; Geng, Y.; Discher, D. E.; Yang, S. *Adv. Mater.* **2006,** *18*, 2905.
28. Rusa, C. C.; Bullions, T. A.; Fox, J.; Porbeni, F. E.; Wang, X. W.; Tonelli, A. E. *Langmuir* **2002,** *18*, 10016.
29. Pozuelo, J.; Mendicuti, F.; Mattice, W. L. *Macromolecules* **1997,** *30*, 3685.
30. Miyake, K.; Yasuda, S.; Harada, A.; Sumaoka, J.; Komiyama, M.; Shigekawa, H. J. *Am. Chem. Soc.* **2003,** *125*, 5080.
31. Ceccato, M.; LoNostro, P.; Baglioni, P. *Langmuir* **1997,** *13*, 2436.
32. Yuen, F.; Tam, K. C. *Soft Matter* **2010,** *6*, 4613.
33. Harada, A.; Kamachi, M. *Macromolecules* **1990,** *23*, 2821.
34. Huang, J.; Ren, L. X.; Zhu, H.; Chen, Y. M. *Macromol. Chem. Phys.* **2006,** *207*, 1764.
35. van de Manakker, F.; Vermonden, T.; van Nostrum, C. F.; Hennink, W. E. *Biomacromolecules* **2009,** *10*, 3157.
36. Liu, J. H.; Sondjaja, H. R.; Tam, K. C. *Langmuir* **2007,** *23*, 5106.
37. Yuan, R. X.; Shuai, X. T. *J. Polym. Sci. Part B-Polym. Phys.* **2008,** *46*, 782.
38. Duan, Q.; Miura, Y.; Narumi, A.; Shen, X.; Sato, S.; Satoh, T.; Kakuchi, T. J. *Polym. Sci. Part a-Polym. Chem.* **2006,** *44*, 1117.
39. Tu, C. W.; Kuo, S. W.; Chang, F. C. *Polymer* **2009,** *50*, 2958.
40. Feng, L.; Hu, J.; Liu, Z.; Zhao, F.; Liu, G. *Polymer* **2007,** *48*, 3616.
41. Jakes, J. *Czechoslovak J. Phys.* **1988,** *38*, 1305.
42. Zimm, B. H. *J. Chem. Phys.* **1948,** *16*, 1093.
43. Ravi, P.; Wang, C.; Tam, K. C.; Gan, L. H. *Macromolecules* **2003,** *36*, 173.
44. Liu, Y.; Zhao, D. Y.; Ma, R. J.; Xiong, D. A.; An, Y. L.; Shi, L. Q. *Polymer* **2009,** *50*, 855.
45. Zhao, C. L.; Winnik, M. A.; Riess, G.; Croucher, M. D. *Langmuir* **1990,** *6*, 514.
46. Sinaga, A.; Hatton, T. A.; Tam, K. C. *Macromolecules* **2007,** *40*, 9064.
47. Li, X.; Li, J.; Leong, K. W. *Macromolecules* **2003,** *36*, 1209.
48. Harada, A.; Li, J.; Kamachi, M. *Macromolecules* **1993,** *26*, 5698.
49. Harada, A.; Li, J.; Kamachi, M. *Nature* **1992,** *356*, 325.
50. Harada, A.; Li, J.; Kamachi, M. J. *Am. Chem. Soc.* **1994,** *116*, 3192.
51. Li, J.; Ni, X. P.; Zhou, Z. H.; Leong, K. W. *J. Am. Chem. Soc.* **2003,** *125*, 1788.
52. Coleman, A. W.; Nicolis, I.; Keller, N.; Dalbiez, J. P. *J. Inclusion Phenomena Mol. Recogn. Chem.* **1992,** *13*, 139.
53. Dai, S.; Tam, K. C. *J. Colloid Interface Sci.* **2005,** *292*, 79.
54. Rekharsky, M. V.; Mayhew, M. P.; Goldberg, R. N.; Ross, P. D.; Yamashoji, Y.; Inoue, Y. J. *Phys. Chem. B* **1997,** *101*, 87.
55. Dormidontova, E. E. *Macromolecules* **2004,** *37*, 7747.
56. Hammouda, B.; Ho, D. L.; Kline, S. *Macromolecules* **2004,** *37*, 6932.
57. Dai, S.; Ravi, P.; Tam, K. C.; Mao, B. W.; Gan, L. H. *Langmuir* **2003,** *19*, 5175.
58. Tang, Y. C.; Ding, Y. W.; Zhang, G. Z. *J. Phys. Chem. B* **2008,** *112*, 8447.
59. Ding, Y. W.; Zhang, G. Z. *J. Phys. Chem. C* **2007,** *111*, 5309.